

基于 PbI_2 的有机-无机杂化化合物的合成和晶体结构

袁国军* 刘光祥 时 超 邵冬生
(南京晓庄学院环境科学学院, 南京 211171)

摘要: 合成得到了 2 个新的有机-无机杂化化合物 $\{(4\text{-CH}_3\text{-Bz-4-Ph-Py})[\text{PbI}_3]\}_n$ (**1**) (其中 4-CH₃-Bz-4-Ph-Py 是 4-甲基苄基-4-苯基吡啶阳离子)和 $\{(4\text{-CF}_3\text{-Bz-4-Ph-Py})[\text{PbI}_3]\}_n$ (**2**) (其中 4-CF₃-Bz-4-Ph-Py 是 4-三氟甲基苄基-4-苯基吡啶阳离子)。对化合物 **1** 和 **2** 进行了元素分析、粉末 X 射线衍射等表征, 并利用 X 射线单晶衍射测定了它们的单晶结构。化合物 **1** 属于正交晶系, $P2_12_12_1$ 空间群; 化合物 **2** 与 **1** 同构。结构研究表明, 化合物 **1** 和 **2** 中, 铅碘八面体通过共边连接方式, 形成 $[\text{Pb}_3\text{I}_9]_n$ 三链, 有机阳离子填充在无机碘化铅链空隙中。

关键词: 碘化铅; 有机-无机杂化化合物; 晶体结构

中图分类号: O614.43*3

文献标识码: A

文章编号: 1001-4861(2017)10-1855-06

DOI: 10.11862/CJIC.2017.225

Syntheses and Crystal Structures of Two Homogeneous Organic-Inorganic Compounds Based on PbI_2

YUAN Guo-Jun* LIU Guang-Xiang SHI Chao SHAO Dong-Sheng

(Department of Applied Chemistry, School of Environmental Science, Nanjing Xiaozhuang University, Nanjing 211171, China)

Abstract: Two homogeneous compounds, $\{(4\text{-CH}_3\text{-Bz-4-Ph-Py})[\text{PbI}_3]\}_n$ (**1**) (4-CH₃-Bz-4-Ph-Py = 4-methylbenzyl-4-phenylpyridinium) and $\{(4\text{-CF}_3\text{-Bz-4-Ph-Py})[\text{PbI}_3]\}_n$ (**2**) (4-CF₃-Bz-4-Ph-Py = 4-trifluoromethylbenzyl-4-phenylpyridinium), have been synthesized and characterized by elemental analysis and single-crystal X-ray diffraction. Compound **1** crystallizes in orthorhombic, space group $P2_12_12_1$, and compounds **1** and **2** are isostructural. Structure analyses reveal that iodoplumbate ion exhibits octahedron topology in compounds **1** and **2**, and all these octahedron topologies form 1D polymeric chain through edge-sharing connecting modes. The organic cation fill in the gap formed by inorganic iodoplumbate polymeric chain. CCDC: 1572362, **1**; 1572361, **2**.

Keywords: lead iodide; organic-inorganic hybrid compounds; crystal structure

0 Introduction

Haloplumbate-based hybrids have been received considerable research interests due to their tunable structures from the discrete mononuclear or polynuclear species (zero-dimensional, 0D) to the infinite variety with higher dimensionality^[1-13] (one-dimensional^[1,3-9],

two-dimensional^[7-11] or three-dimensional^[2]; hereafter abbr. as 1D, 2D and 3D, respectively) and the wide range of novel physical properties, beneficial in optics^[14-18] and electronics^[19-21].

In the context of haloplumbate-based hybrids, the perovskite-type ones have attracted tremendous research interest. The 3D haloplumbate-based perovskites,

收稿日期: 2017-04-22。收修改稿日期: 2017-08-02。

江苏省自然科学基金(No.BK20170145)、江苏省教育厅高校自然科学研究面上项目(No.15KJB150019)和江苏省高等学校大学生实践创新训练计划(No.201511460027Y)资助。

*通信联系人。E-mail: ahchljy@163.com

$\text{CH}_3\text{NH}_3\text{PbI}_{3-x}\text{Cl}_x$, with much lower exciton binding energies and intense light absorption over the whole visible light region have been employed as absorbers in solar cells. It is remarkable that the records of certified power conversion efficiencies have been constantly updated and over merely a few years, the power conversion efficiency has been enhanced to 20%^[19]. Most recently, the $\text{CH}_3\text{NH}_3\text{PbI}_{3-x}\text{Cl}_x$ perovskites have been found to show amazing bipolar and bistable resistive switching behavior with small on-off voltage lower than 1.0 V in a simple metal-dielectric-metal capacitor configuration device memory field^[22]. The 2D haloplumbate-based hybrids, $(N\text{-MEDA})\text{-}[\text{PbBr}_{4-x}\text{Cl}_x]$ ($N\text{-MEDA}$ = N -methylethane-1,2-diammonium, $x=0\sim 1.2$), are single-phase white-light emitters, and their broad-band emission across the entire visible spectrum arises from corrugated lead halide sheets. Interestingly, the emission is tunable through halide substitution to afford both “warm” and “cold” white light in such haloplumbate-based wide-band gap semiconductors^[14]. The 1D iodoplumbate-based hybrids were reported to display ferroelectricity, wherein the polarization is switchable under an alternating current electrical field^[23].

In addition, a 3D open-framework hybrid, $[(\text{EDAMP})_2(\text{Pb}_7\text{I}_{18})\cdot 4\text{H}_2\text{O}]_n$ ($\text{EDAMP}=\text{Et}_2\text{NHC}_6\text{H}_4\text{CH}_2\text{C}_6\text{H}_4\text{NHEt}_2$), in which the inorganic framework is built from purely octahedral PbI_6 units and behaves as a quantum-wire array, shows a fascinating wavelength-dependent photochromic behavior^[24]. Its color changes from yellow to olive green under illumination with $\lambda=500$ nm light and further to dark green with light of $\lambda < 500$ nm. Most interestingly, the reversion of the color for the hybrid can be accomplished by heating, indicating that this hybrid possesses switchable photochromic nature. It is well known that a material with switchable functionality through external stimuli, such as thermally-triggered, irradiation-induced and applied pressure, is very useful for application in the fields of sensors, memory and data storage^[25-28].

In this study, we report the syntheses, crystal structures and thermal properties of two iodoplumbate-based hybrids, $\{(\text{4-CH}_3\text{-Bz-4-Ph-Py})[\text{PbI}_3]\}_n$ (**1**) and $\{(\text{4-}$

$\text{CF}_3\text{-Bz-4-Ph-Py})[\text{PbI}_3]\}_n$ (**2**).

1 Experimental

1.1 Materials and general methods

All chemicals and solvents were reagent grade and used without further purification. Elemental analyses for C, H and N were performed with an Elementar Vario EL III analytic instrument. Powder X-ray diffraction (PXRD) data for **1** and **2** were collected on a Rigaku/max-2550 diffractometer with Cu $K\alpha$ radiation ($\lambda=0.154$ 18 nm) at room temperature with acceleration voltage of 40 kV and current of 40 mA. The data were collected in the 2θ range from 5° to 50° . Electric spray ionization mass spectra were performed on LCO Fleet ESI Mass Spectrometer.

1.2 Synthesis of $\{(\text{4-CH}_3\text{-Bz-4-Ph-Py})[\text{PbI}_3]\}_n$ (**1**)

$[\text{4-CH}_3\text{-Bz-4-Ph-Py}]\text{Br}$. 4-Methylbenzyl bromide ($[\text{4-CH}_3\text{-Bz}]\text{Br}$, 370 mg, 2 mmol) and 4-Phenylpyridine (4-Ph-Py)(310 mg, 2 mmol) were mixed under stirring in acetone (25 mL) at 55°C and the formed purple microcrystal product was filtered off, washed with acetone and then dried in vacuum at room temperature to give 670 mg of $[\text{4-CH}_3\text{-Bz-4-Ph-Py}]\text{Br}$ (Yield: 92%). Elemental analysis calculated for $\text{C}_{19}\text{H}_{18}\text{NBr}(\%)$: C, 67.07; H 5.33; N, 4.12. Found(%): C, 67.02, H, 5.30, N, 4.09. MS-ESI: $m/z=260.25$ ($[\text{4-CH}_3\text{-Bz-4-Ph-Py}]^+$).

$\{(\text{4-CH}_3\text{-Bz-4-Ph-Py})[\text{PbI}_3]\}_n$ (**1**). A mixture of $[\text{4-CH}_3\text{-Bz-4-Ph-Py}]\text{Br}$ and KI and PbI_2 with a molar ratio of 1:1:1 in DMF (25 mL) was placed in an oven and slowly evaporated at 55°C for 10~14 days to produce light yellow needle-shaped crystals in ca. 95% yield. Elemental analysis calculated for $\text{C}_{38}\text{H}_{36}\text{N}_2\text{Pb}_3\text{I}_8(\%)$: C, 23.40; H, 1.86; N, 1.44. Found(%): C, 23.36, H, 1.84, N, 1.41.

1.3 Synthesis of $\{(\text{4-CF}_3\text{-Bz-4-Ph-Py})[\text{PbI}_3]\}_n$ (**2**)

$[\text{4-CF}_3\text{-Bz-4-Ph-Py}]\text{Br}$. The synthesis of $[\text{4-CF}_3\text{-Bz-4-Ph-Py}]\text{Br}$ was similar with $[\text{4-CH}_3\text{-Bz-4-Ph-Py}]\text{Br}$ except 4-trifluoromethylbenzyl bromide ($[\text{4-CF}_3\text{-Bz}]\text{Br}$, 478 mg, 2 mmol) was used instead of $[\text{4-CH}_3\text{-Bz}]\text{Br}$. Yield: 92%. Elemental analysis calculated for $\text{C}_{19}\text{H}_{15}\text{F}_3\text{NBr}(\%)$: C, 57.89; H 3.84; N, 3.55. Found(%): C, 57.86, H, 3.82, N, 3.53. MS-ESI: $m/z=314.25$ ($[\text{4-CF}_3\text{-}$

Bz-4-Ph-Py]⁺).

{(4- CF_3 -Bz-4-Ph-Py)[PbI_3]}_n (**2**). The synthesis of **2** was similar with **1** except [4- CF_3 -Bz-4-Ph-Py]Br was used instead of [4- CH_3 -Bz-4-Ph-Py]Br. Yield: ca. 95%. Elemental analysis calculated for $\text{C}_{38}\text{H}_{30}\text{F}_6\text{N}_2\text{Pb}_3\text{I}_8$ (%): C, 20.15; H 1.33; N, 1.24. Found(%): C, 20.12, H, 1.30, N, 1.21.

1.4 X-ray crystallography

The single-crystal X-ray diffraction data for **1** and **2** were collected at 296(2) K with graphite monochromated Mo $K\alpha$ ($\lambda=0.071\ 073\ \text{nm}$) on a CCD area detector (Bruker-SMART). Data reductions and absorp-

tion corrections were performed with the SAINT and SADABS software packages^[29], respectively. Structures were solved by a direct method using the SHELXL-2014 software package^[30]. The non-hydrogen atoms were anisotropically refined using the full-matrix least-squares method on F^2 . All hydrogen atoms were placed at the calculated positions and refined riding on the parent atoms. The details about data collection, structure refinement and crystallography are summarized in Table 1.

CCDC: 1572362, **1**; 1572361, **2**.

Table 1 Crystallographic and structure refinement data for **1** and **2**

Compound	1	2
Formula weight	848.26	902.23
Space group	$P2_12_12$	$P2_12_12$
Crystal system	Orthorhombic	Orthorhombic
a / nm	2.164 1(4)	2.175 6(3)
b / nm	2.407 9(4)	2.445 0(4)
c / nm	0.451 37(8)	0.455 10(8)
V / nm^3	2.352 1(7)	2.420 8(7)
Z	2	2
$D_c / (\text{g} \cdot \text{cm}^{-3})$	3.046	3.108
$F(000)$	1 896	1 992
μ / mm^{-1}	15.989	15.560
θ range for data collection / ($^\circ$)	1.936~25	1.911~25.009
Index ranges	$-25 \leq h \leq 25, -28 \leq k \leq 28, -5 \leq l \leq 5$	$-25 \leq h \leq 25, -29 \leq k \leq 25, -5 \leq l \leq 5$
R_{int}	0.077 0	0.072 8
Independent reflection, restraint, parameter	4 148, 168, 221	4 264, 88, 259
Refinement method	Full-matrix least-squares on F^2	
Goodness of fit on F^2	1.086	1.051
$R_1, wR_2^* [I > 2\sigma(I)]$	$R_1=0.087\ 4, wR_2=0.225\ 4$	$R_1=0.081\ 1, wR_2=0.201\ 0$
R_1, wR_2^* (all data)	$R_1=0.095\ 1, wR_2=0.230\ 0$	$R_1=0.089\ 2, wR_2=0.205\ 3$
$(\Delta\rho)_{\text{max}}, (\Delta\rho)_{\text{min}} / (\text{e} \cdot \text{nm}^{-3})$	2 481, -3 672	2 492, -2 789

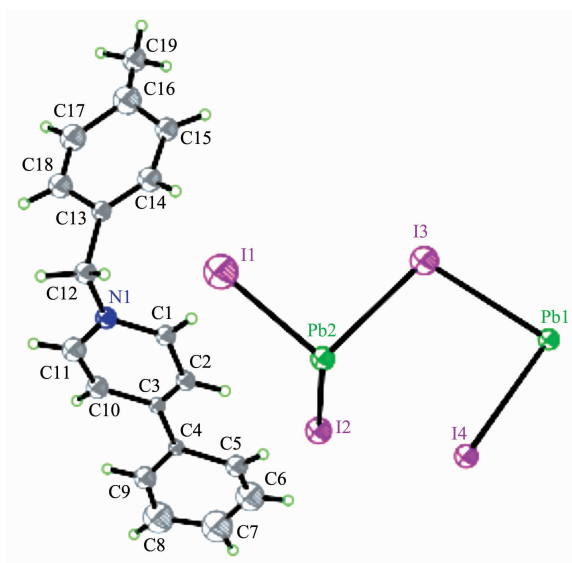
$$^*R_1 = \sum \|F_o\| - |F_c| / \sum \|F_o\|, wR_2 = [\sum w(F_o^2 - F_c^2)^2 / \sum w(F_o^2)^2]^{1/2}$$

2 Results and discussion

2.1 Description of crystal structure

Compound **1** crystallizes in the $P2_12_12$ space group at room temperature. The asymmetric unit, as shown in Fig.1, consists of one Pb^{2+} ion and three different I^- anions together with one 4- CH_3 -Bz-4-Ph-Py cation. The Pb^{2+} ion locates at an inversion center

and is coordinated with six I^- to form the slightly distorted PbI_6 octahedron. The Pb-I lengths range from 0.282 48(46) to 0.358 35(27) nm and the I-Pb-I angles fall within the range of $80.393(74)^\circ \sim 171.711(108)^\circ$ at 296 K, these geometry parameters within the coordination octahedron are comparable to other iodoplumbates. Three different I^- ions adopt the μ_3 -bridged model to connect three neighboring Pb^{2+} ions. The



Hydrogen atoms are non-labeled for clarity

Fig.1 ORTEP view of **1** with thermal ellipsoids at 30% probability level

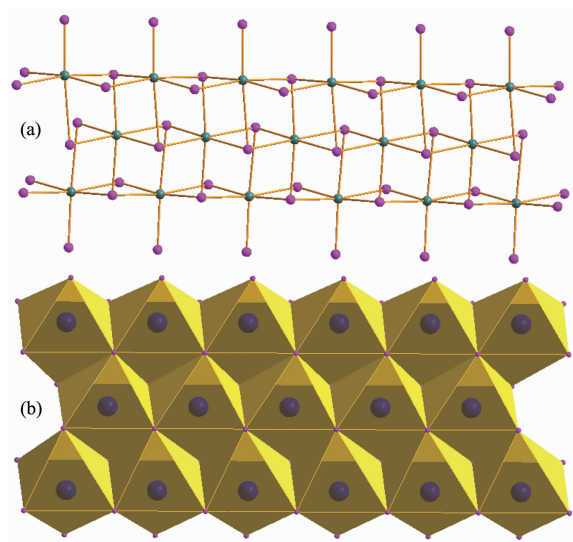


Fig.2 Edge-sharing octahedral chain of $[\text{Pb}_3\text{I}_9]_n$ in compounds **1** and **2**: (a) Stick and ball model; (b) polyhedron model

adjacent PbI_6 coordination octahedral are connected together via the edge-sharing mode to form a uniform $[\text{Pb}_3\text{I}_9]_n$ chain along the a -axis direction (Fig.2).

The cation is composed of a 4-phenylpyridine and a 4-methylbenzyl, the neighboring cations are aligned into quadrilateral-shaped 1D channels, and the inorganic $[\text{Pb}_3\text{I}_9]_n$ chains reside in the channels (Fig.3). Charged-assisted H-bonding interactions appear between the CH_2 groups in the cations and the I^- ions in the inorganic chains. Compound **2** (Fig.4~5) is

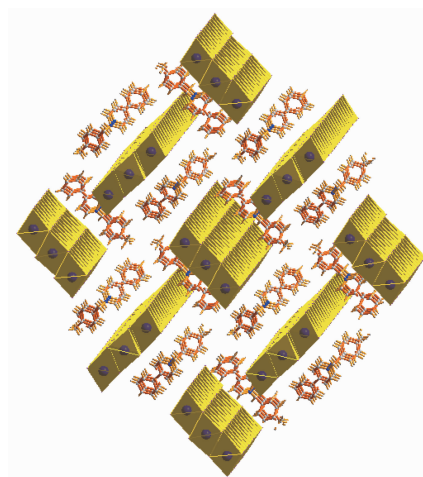
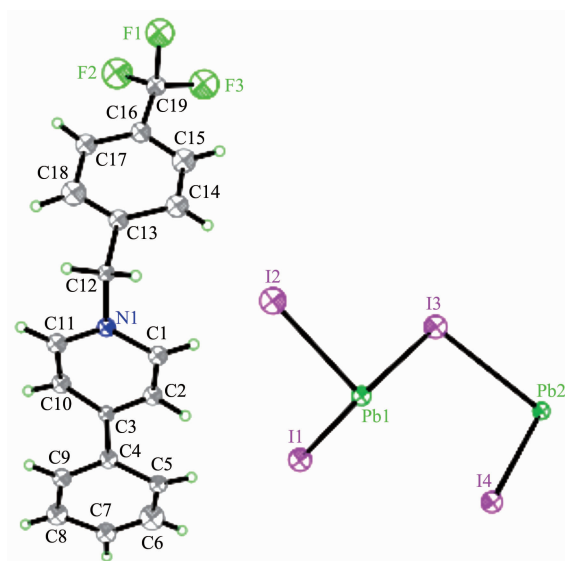


Fig.3 Molecular packing diagram for compound **1**



Hydrogen atoms are non-labeled for clarity

Fig.4 ORTEP view of **2** with thermal ellipsoids at 30% probability level

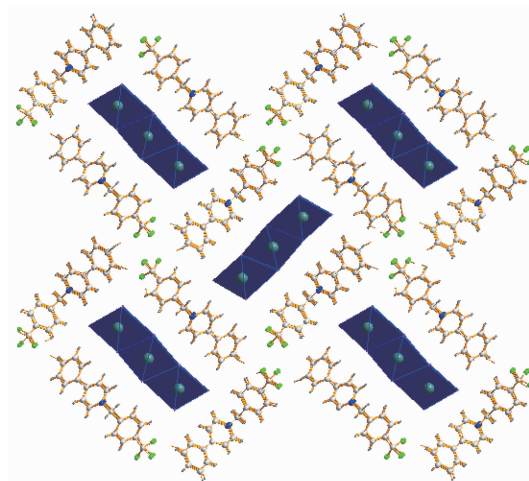


Fig.5 Molecular packing diagram for compound **2**

isostructural with compound **1**.

2.2 Thermal stability and powder X-ray diffraction (PXRD)

To examine the thermal stability of compounds **1** and **2**, TG analyses were carried out (Fig.7). The TG study of compound **1** shows a weight loss of 26.09% from 27 to 340 °C, corresponding to the loss of cation. Then the compound starts to decomposes at 340 °C, corresponding to the loss of anion. In the case of compound **2**, a weight loss of 31.47% from 19 to 345 °C, corresponding to the loss of cation. Then the compound **2** starts to decompose at 345 °C, corresponding to the loss of anion.

Powder X-ray diffraction analysis (PXRD) experiments were carried out for **1** and **2** at room

temperature to characterize their purity. As shown in Fig.7, the measured peak positions closely match the simulated peak positions, indicative of pure products.

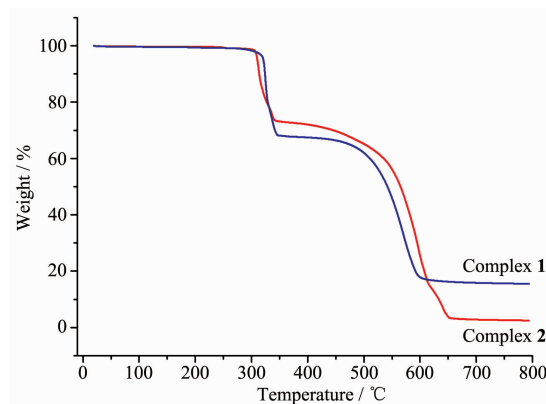


Fig.6 TGA curves of compounds **1** and **2**

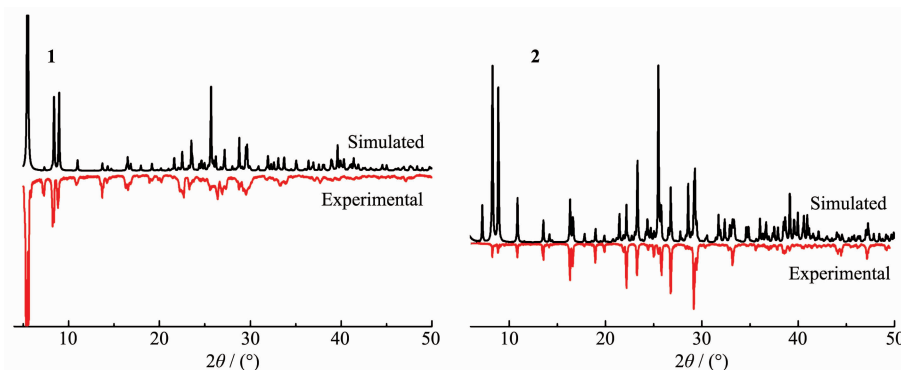


Fig.7 PXRD patterns of compounds **1** and **2**

References:

- [1] Zhao S P, Ren X M. *Dalton Trans.*, **2011**,**40**:8261-8272
- [2] Krautscheid H, Vielsack F. *Angew. Chem. Int. Ed.*, **1995**,**34**: 2035-2037
- [3] Krautscheid H, Lode C, Vielsack F, et al. *J. Chem. Soc., Dalton Trans.*, **2001**:1099-1104
- [4] Tang Z, Guloy A M. *J. Am. Chem. Soc.*, **1999**,**121**:452-453
- [5] Liu J J, Guan Y F, Jiao C, et al. *Dalton Trans.*, **2015**,**44**: 5957-5960
- [6] Zhang Z J, Xiang S C, Zhang Y F, et al. *Inorg. Chem.*, **2006**, **45**:1972-1977
- [7] She Y J, Zhao S P, Ren X M, et al. *Inorg. Chem. Commun.*, **2014**,**46**:29-32
- [8] Tong Y B, Ren L T, Ren X M, et al. *Dalton Trans.*, **2015**,**44**: 17850-17858
- [9] Duan H B, Yu S S, Ren X M, et al. *Dalton Trans.*, **2016**,**45**: 4810-4818
- [10] Lemmerer A, Billing D G. *CrystEngComm*, **2012**,**14**:1954-1966
- [11] Willett R D, Maxcy K R, Twamley B. *Inorg. Chem.*, **2002**, **41**:7024-7030
- [12] SUN Cai(孙财), WANG Ming-Sheng(王明盛), GUO Guo-Cong(郭国聪). *Proceedings of Ninth Chinese Inorganic Chemistry Conference*(全国第九届无机化学学术会议论文集). Nanchang:[s.n.], **2015**:315
- [13] Fujian Institute of Research on the Structure of Matter(福建物质结构研究所). *Bulletin of the Chinese Ceramic Society* (硅酸盐通报), **2016**,**2**:143
- [14] Dohner E R, Hoke E T, Karuadasa H I. *J. Am. Chem. Soc.*, **2014**,**136**:1718-1721
- [15] Wehrenfenging C, Liu M, Snaith H J, et al. *J. Phys. Chem. Lett.*, **2014**,**5**:1300-1306
- [16] Guloy A M, Tang Z J, Miranda P B, et al. *Adv. Mater.*, **2001**, **13**:833-837
- [17] Fujisawa J I, Ishihara T. *Phys. Rev. B: Condens. Matter Mater. Phys.*, **2004**,**70**:113024-113203
- [18] Liu G N, Shi J R, Han X J, et al. *Dalton Trans.*, **2015**,**44**:

- 12561-12575
- [19]Yang W S, Noh J H, Jeon N J, et al. *Science*, **2015**,**348**: 1234-1237
- [20]Liu M, Johnston M B, Snaith H J. *Nature*, **2013**,**501**:395-398
- [21]Xing G, Mathews N, Sun S, et al. *Science*, **2013**,**18**:344-347
- [22]Yoo E J, Lyu M, Yun J H, et al. *Adv. Mater.*, **2015**,**27**: 6170-6175
- [23]Zhao H R, Li D P, Ren X M, et al. *J. Am. Chem. Soc.*, **2010**,**132**:18-19
- [24]Zhang Z J, Xiang S C, Guo G C, et al. *Angew. Chem., Int. Ed.*, **2008**,**47**:4149-4152
- [25]Maldonado P, Kanungo S, Saha-Dasgupta T, et al. *Phys. Rev. B: Condens. Matter Mater. Phys.*, **2013**,**88**:020408
- [26]Kahn O, Martinez C J. *Science*, **1999**,**279**:44-48
- [27]Liang J, Chen Z, Xu L, et al. *J. Mater. Chem. C*, **2014**,**2**: 2243-2250
- [28]Dong X Y, Li B, Ma B B, et al. *J. Am. Chem. Soc.*, **2013**, **135**:10214-10217
- [29]*SMART* and *SAINT*, Siemens Analytical X-ray Instrument Inc., Madison, WI, **1996**.
- [30]Sheldrick G M. *Acta Crystallogr. Sect. C*, **2015**,**C71**:3-8